ARTICLE NO. 78-1283R

Active Local Vibration Isolation Applied to a Flexible Space Telescope

C.E. Kaplow*
Hughes Aircraft Co., Culver City, Calif.
and
J.R. Velman†
Hughes Aircraft Co., El Segundo, Calif.

Two problems in the design of large space telescopes are the effects of vibrating equipment on optical alignments and the instabilities that may result from flexible coupling between the attitude sensors and actuators. This paper explores a design concept where the spacecraft is divided into two modules: a quiet optics module containing the attitude sensors and a vibrating equipment module containing the attitude actuators. The modules are connected by active isolation devices that transmit low-frequency attitude control forces but attenuate higher-frequency disturbances. Performance analyses were based on a fifty-degree-of-freedom spacecraft model with nine active control loops.

Introduction

TWO important problems in the design of large space telescopes are the effects of vibrating equipment on payload performance and the instabilities that may result from flexible coupling between attitude sensors and actuators. The possible sources of vibrations include the attitude control system which may use large momentum wheels, control moment gyros, or reaction jets. These vibrations, if coupled into the structural dynamics of a flexible optical system, can seriously disturb the image quality. The interaction instability problem arises through the fact that attitude sensors may be located at some distance in the structure from the attitude control actuators. This is particularly true with optical systems where the performance depends on accurately pointing and stabilizing a telescope line of sight and the attitude error signals are derived from the image. This was the case, for example, in OSO-I, where a potential control instability problem was solved by a notched filter approach as described in Ref. 1.

In general, when it is required to maintain the alignment of a large, compliant spacecraft structure within very small tolerances, there are two ways to proceed. One alternative is to implement a high-performance (wide bandwidth) control system that can operate in the expected dynamic disturbance environment and attenuate the disturbances to an acceptable level. A second alternative is to isolate the disturbances from the critical parts of the spacecraft so that a high-performance control system for the critical structure is not necessary. The selection of either one or the other approach depends mainly on the maneuver or scanning requirements. In general, the structural deformations caused by maneuvering or slewing a large spacecraft are of far greater importance than the disturbance produced by onboard rotating machinery. A maneuvering spacecraft is therefore required to be relatively rigid, and this precludes the possibility of partially decoupling the major disturbance sources from the critical parts of the structure. The present paper considers only a non-maneuvering spacecraft so that the disturbance isolation approach is possible.

The use of active or passive vibration isolation has a long history and an extensive literature. Reference 2 provides analyses of the isolation characteristics achievable using various nonlinear damping laws. The active isolation system described herein could easily be adapted to implement any of these characteristics should it be desirable. In Ref. 3, a vibration isolator of the type discussed here is interpreted in terms of optimal control. Reference 4 provides a more complete investigation of the choice of isolator parameters to optimize performance relative to a cost functional. Each of these references contain extensive bibliographical information.

Figure 1 illustrates a spacecraft configuration that was investigated for this study. The optics structure is a large telescope which comprises most of the physical volume of the spacecraft and much of the mass. The vibrating equipment module contains the attitude control and other vibrating equipment. The two are connected by six single-degree-of-freedom isolator mechanisms. The second section of the paper describes the isolation concept in detail and investigates the properties and performance of the isolation concept in terms of a two-degree-of-freedom model. In the third section, the full system model used to validate the isolation concept is described. The system model included a 52 mode flexible optical system; the attitude control loops were independent, and the six isolation control loops were each independent. The results of the system study are presented in the fourth section. The results include frequency response of the line of sight to disturbances on the vibrating equipment module and the time responses for both an attitude transient and a sinusoidal disturbance on the vibrating equipment module.

Active Disturbance Isolation

The decision to isolate disturbances from the critical parts of the optical support structure leads naturally to the "dirty box" isolation concept. In this approach, all disturbance sources are mounted on a separate vibrating equipment module called the dirty box. The dirty box is then isolated

Presented as Paper 78-1283 at the AIAA Guidance and Control Conference, Palo Alto, Calif., Aug. 7-9, 1978; submitted Sept. 12, 1978; revision received Oct. 16, 1979.

Index categories: Spacecraft Dynamics and Control; Spacecraft Simulation; Spacecraft Configurational and Structural Design (including Loads).

*Section Head, Electro-Optical & Data Systems Group. Member AIAA.

†Associate Department Manager, Space & Communications Group. Member AIAA.

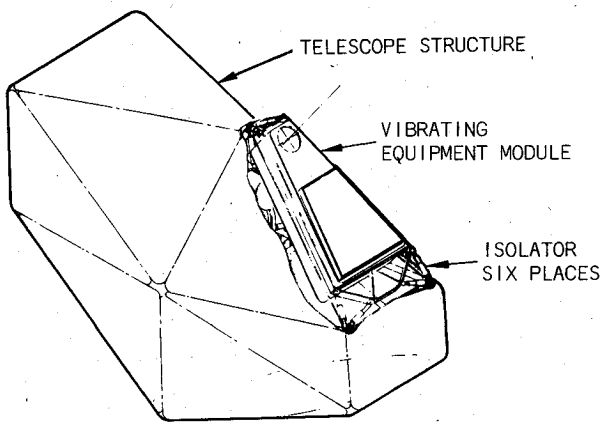

Fig. 1 System dynamics model.

from the clean or critically aligned portions of the structure.

Isolation of the dirty box can conceivably be accomplished by three general methods: 1) passive isolation, 2) active isolation using local error sensing; and 3) active isolation using a global modal control approach.

Passive isolation employs purely passive elements such as springs and dashpots connected across the interface between the clean and dirty structures. Active isolation with local error sensing employs actively controlled force actuators in addition to passive elements. The actuators are controlled by inertial transducers mounted at the points on the clean structure where the actuators are attached. Active isolation using the global modal control approach provides a policy for driving the actuators based on the modal behavior of the entire spacecraft. In this approach, the standard methods of linear-quadratic-Gaussian optimal control theory can be applied to the design of a control system that can actively damp selected structural modes. The modes that are not actively damped are assumed to have adequate inherent structural damping.[5]

The modal control approach offers potential high performance but has the disadvantage of great complexity. In practice, a number of difficulties would be encountered. First of all, the control system would require measurements of the amplitudes of the modes which are to be controlled. The modal amplitudes could be measured with relative ease if the modes were widely separated in frequency. In fact, however, structures are likely to exhibit clustering of modes where the frequency separation is very small.

A second difficulty with the optimal control approach is that the realistic representation of a large structure requires processing a great many modes. The successful application of optimal control theory to large space structures requires judicious simplification of the system model.

The approach presented in this paper for dirty box isolation is the active technique using local error sensing. A system implemented on this basis has an inherent simplicity and appears to be capable of meeting reasonable performance levels.

Active Isolation Concept

The general isolation concept considered here is shown in Fig. 2. Two elements are shown connected across the isolation interface between the clean and dirty structures: an actively controlled actuator producing force F_a and a spring with stiffness k. An accelerometer is mounted on the clean structure at the point where the force actuator is attached.

In order to evaluate the merits of a particular isolation method, it is necessary to decide what constitutes the ideal isolation system. Since the control moment gyros (CMG's), reaction wheels, and/or thrusters that produce spacecraft attitude stabilization are themselves a major source of disturbance forces, they should be mounted in the dirty box. In order to produce attitude stabilization, it is necessary, therefore, to transmit low bandwidth forces and motions across the isolation interface. This is illustrated in Fig. 3 which shows the motion transfer ratio (clean motion to dirty motion) as a function of frequency. Ideally, the motion transfer should be unity up to some frequency ω_n corresponding to the isolator cutoff frequency. Beyond this frequency, the ideal isolator would provide infinite attenuation. The ideal isolation characteristic, therefore, is flat up to the frequency ω_n and then breaks vertically downward. The ideal isolation characteristic provides a standard against which various physically realizable schemes can be compared.

The basic active isolator proposed in this paper has a characteristic described by the active isolation curve of Fig. 3. The curve is flat until it reaches the vicinity of the frequency ω_n. The curve then breaks downward with a slope of -40 dB/decade.

The isolation characteristic for a purely passive isolator consisting of a dashpot in parallel with a spring is also shown in Fig. 3. Two curves are drawn corresponding to two values of damping. In each case, the isolator has a resonance at the frequency ω_n. On the curve corresponding to the higher value of damping, the resonant peak is less pronounced. However, the higher damping produces a poorer attenuation at high

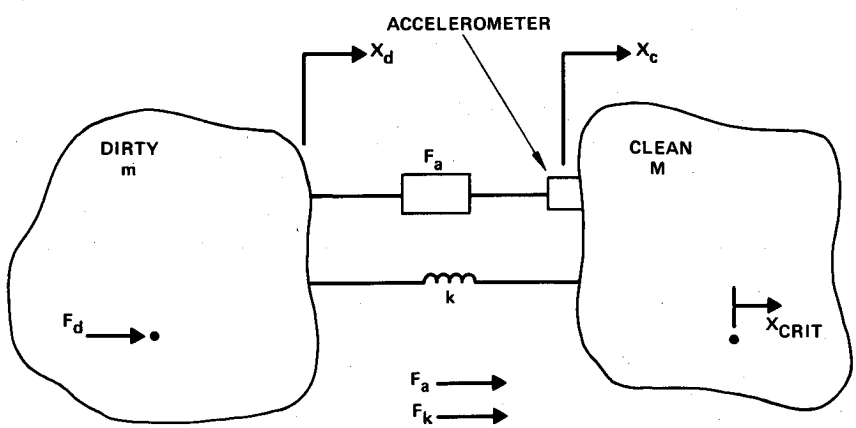

Fig. 2 Active isolation concept.

$$\frac{X_d(s)}{F_d(s)} = G_d(s) = \frac{1}{ms^2} \qquad \frac{X_d(s)}{-F_a(s) - F_k(s)} = G_m(s) = \frac{1}{ms^2} \qquad \frac{X_c(s)}{F_a(s) + F_k(s)} = G_M(s) = \frac{1}{Ms^2}$$

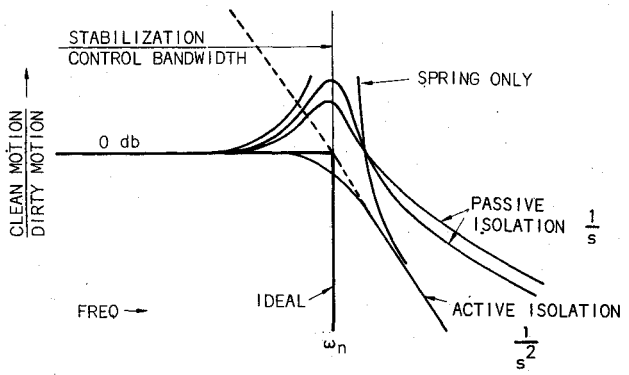

Fig. 3 Comparison of isolation methods.

frequencies. There is a tradeoff, therefore, when passive isolation is used. A compromise must be made between damping of the resonance (at frequency ω_n) and high-frequency attenuation. Visual inspection of accurately plotted passive isolation curves indicates that the best damping ratio would be about 0.2. It should also be noted that the passive isolation curves break downward with a slope of -20 dB/decade regardless of the specific value of damping selected.

In summary, Fig. 3 reveals the two primary advantages of the active isolator compared to the passive isolator:

1) The active isolator eliminates the resonant peak at frequency ω_n.

2) The active isolator provides -40 dB/decade of high-frequency attenuation, while the passive isolator provides only -20 dB/decade.

Figure 3 also shows the isolation characteristic for a simple spring without any kind of damping device. It can be seen that the spring curve is coincident with the active isolation curve at low and high frequencies. However, at the frequency ω_n, the spring curve has an infinite resonance. Clearly, the function of the force actuator in the active isolation method is to provide a damping of this resonance. The force actuator provides the required damping without disturbing the desired rapid high-frequency attenuation.

Active Isolation Control System

The method of controlling the force actuator in the active isolator is shown in Fig. 4. The symbols used in the figure are defined as follows:

x_c	= position of clean side of isolator
x_d	= position of dirty side of isolator
x_{crit}	= position of critical point of clean structure
k	= isolator spring stiffness
K_c	= servo forward gain
M	= mass of clean structure
m	= mass of dirty structure
$G_M(s)$, $G_{crit}(s)$	= transfer functions representing dynamics of clean structure
$G_m(s)$, $G_d(s)$	= transfer functions representing dynamics of dirty structure
$G_c(s)$	= servo loop compensation

The acceleration of the clean structure $\ddot{x}_c$ is measured by the accelerometer. The actuator force F_a is equal to the accelerometer signal multiplied by the servoloop gain and compensation.

The servoloop compensation is selected to be a simple integration, $G_c(s) = 1/s$. It can be shown using classical methods that the integral compensation provides an unconditionally stable control loop.

If it is assumed that the clean and dirty structures are rigid bodies, the relationship between the clean and dirty motion has the form of a low-pass mechanical filter.

$$\frac{x_c}{x_d} = \left(\frac{M}{k}s^2 + \frac{K_c}{k}s + 1\right)^{-1}$$

The isolator cutoff frequency just implied is $\omega_n = \sqrt{k/M}$. The servoelectronic gain K_c is chosen to provide a damping ratio of unity for the quadratic poles of the transfer function.

Spacecraft Attitude Control

To verify the usefulness of the isolation concept, it is necessary to consider the effect of including the isolator dynamics within the spacecraft attitude control loop. It is envisioned that the attitude control actuators are mounted on the dirty side of the interface, while the attitude measurement sensors are on the clean side. The isolator dynamics are therefore included in the forward path of the spacecraft attitude control loop.

Figure 5 shows a model of a simple attitude control loop employing a single isolator. The isolator dynamics shown within the dotted box of the figure are obtained by manipulation of the block diagram of Fig. 4.

The attitude control sensor compares the angular position of the optical structure (corresponding to the line of sight) with a desired or reference angle and determines an angular position error. A control torque is then applied on the dirty side of the isolation interface to null out the angular error. As far as the local dynamics at the attachment points of a single isolator are concerned, the attitude control loop appears to operate on a translational basis as shown in Fig. 5. The attitude control sensor provides a signal x_E that represents a

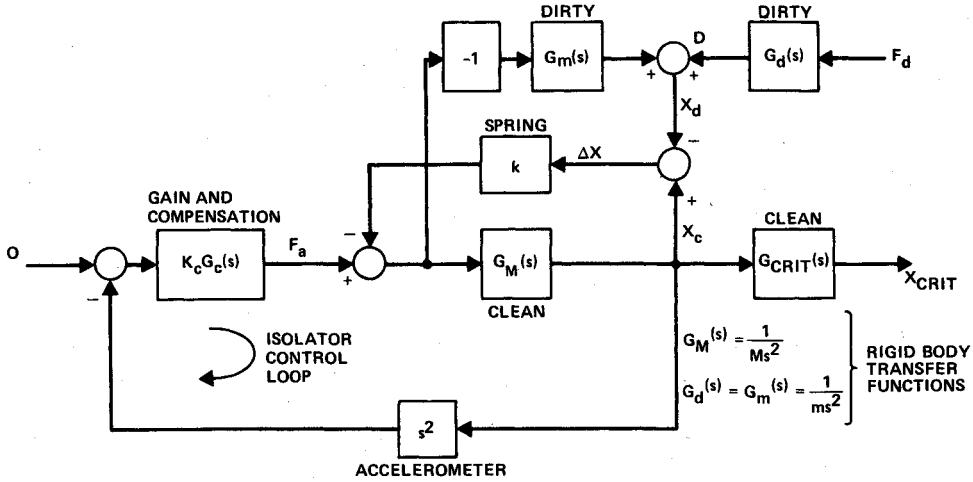

Fig. 4 Dynamic model of isolator.

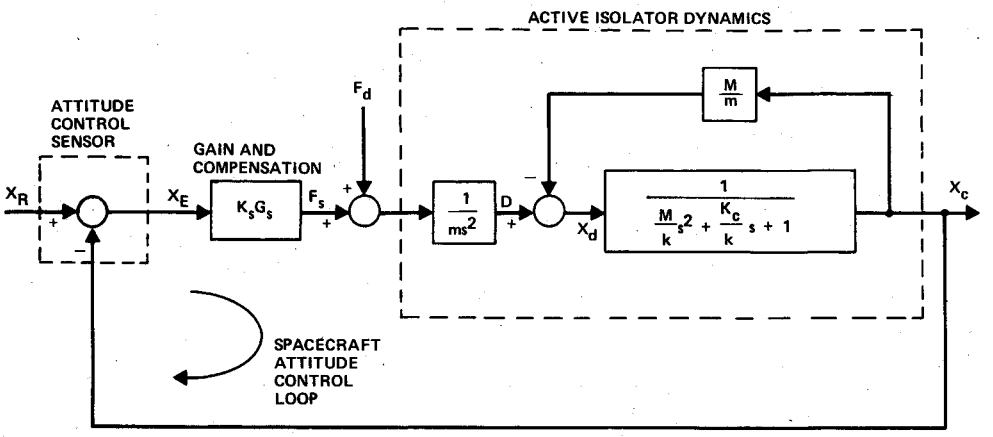

Fig. 5 Spacecraft attitude control loop.

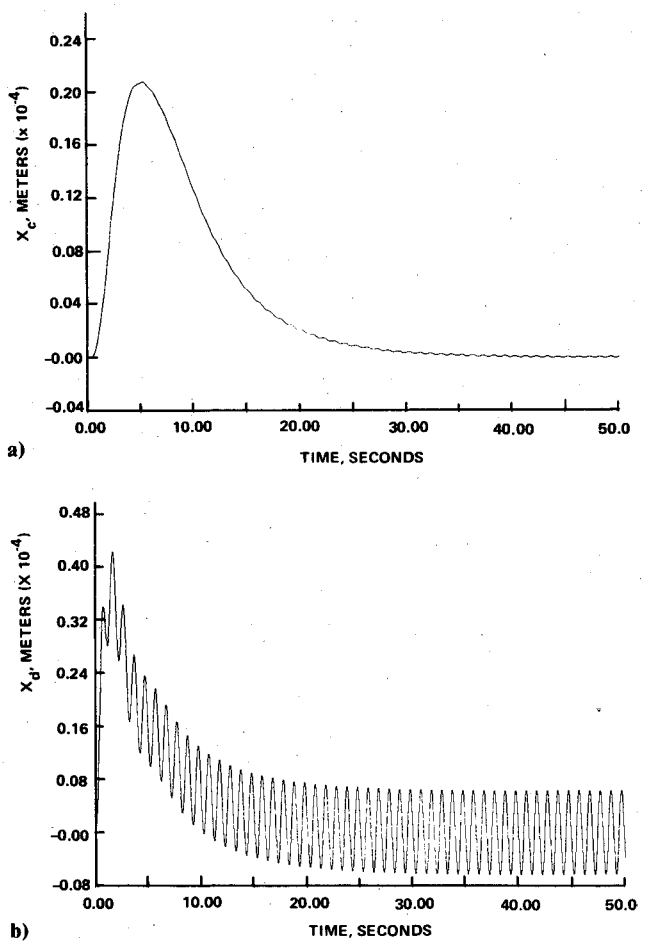

Fig. 6 Active isolator performance for a) clean and b) dirty motion.

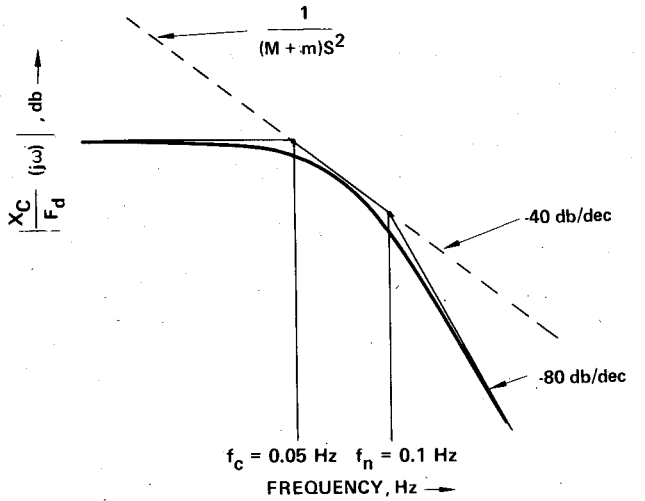

Fig. 7 Relationship between clean structure position and force disturbance.

translational position error at the point of isolator attachment. The attitude control actuators produce a force F_s applied to the dirty side of the isolation interface. The unwanted disturbance force F_d enters the loop at the same point as F_s so that the total force applied to the dirty box is the sum of both the control and disturbance forces.

Typical simulation results for the model of Fig. 5 are shown in Fig. 6. The isolator cutoff frequency was set at 0.1 Hz, and the attitude control loop bandwidth (open loop crossover frequency) was 0.05 Hz. The curves of Fig.6 show the isolator performance in attenuating a force disturbance of 1 N at a frequency of 1 Hz. Both the turn-on transient and the steady-state behavior can be seen. The attitude control loop is stable, and the isolator provides an attenuation that is exactly what would be predicted from theory.

The relationship between the clean structure position x_c and the force disturbance F_d can be derived from Fig. 5. This relationship is plotted in Fig. 7. The asymptotic curve is flat out to the frequency f_c (the bandwidth of the attitude control loop). The curve then breaks downward with a slope of -40 dB/decade. At the frequency f_n (the isolator cutoff frequency), a second break occurs so that the high-frequency slope is -80 dB/decade. Thus, the active isolator provides 40 dB/decade of high-frequency attenuation compared to a system with a rigidly attached vibrating equipment module.

An Optimal Control Interpretation of Active Isolation

In Ref. 3, a vibration isolator of this type is discussed and referred to as a "skyhook damper." There, the velocity $\dot{x}_d$ was taken to be Gaussian white noise, and only the dynamics of the clean box were included in the plant dynamics equations. By making the change of variables $q_1 = \dot{x}_c$, $q_2 = (x_c - x_d)$, and solving for the optimal control using the cost function

$$J = E\left[\int_0^T (c_1 q_1^2 + c_2 q_2^2 + bu^2)\,dt\right]$$

one obtains a closed-loop system

$$\dot{q}_1 = (1/m)u \qquad \dot{q}_2 = q_1 + \dot{x}_d$$

$$u = [k_1(t)q_1 + k_2(t)q_2]$$

The steady-state solution, after changing back to the original variables, is

$$\ddot{x}_c = (-1/m)\,[b\dot{x}_c + k(x_c - x_d)]$$

This is the equation of motion of a mass connected to the dirty box by a spring, to inertial space by an ordinary dashpot, and explains the designation "skyhook damper." This provides an interesting interpretation of the isolator in terms of optimal control theory. The present analysis differs from that of the reference in that the dynamics of the dirty box are included in the plant equations.

Spacecraft Model

Figure 1 shows the system configuration that was used to test the isolation concept with a realistically complicated representation of a space optical system. The optics was coupled to the vibrating equipment module or dirty box by means of six active isolators located as shown in the figure. By proper geometric alignment of these one-degree-of-freedom supports, the full six degrees of freedom of relative motion between the optics and the dirty box can be controlled. The three attitude degrees of freedom were controlled by three independent attitude control channels with the inertial measurement being done on the optics side of the spacecraft and the control torques being applied on the dirty box. The dirty box itself was modeled as a rigid structure.

Figure 8 shows the optical system which comprised the flexible part of the spacecraft. The telescope includes three mirrors and an image plane. The mirrors were modeled as plates in the structural model. The supports between the mirrors are combinations of compression spokes and tension cables. The line-of-sight error depends on the translations of the three mirrors relative to the image plane as well as the orientations of the three mirrors. For this reason, it was necessary in the system model to keep a representation which permitted the determination of the orientations and positions of the three mirrors. In calculating the line-of-sight error, a matrix of sensitivity of two components of line-of-sight error to these twenty-one degrees of freedom was used.

Initially, the optics was represented by a 130 node finite-element model. This model was subjected to a structural analysis by a Stardyne program, and the mode shapes were calculated for natural frequencies up to 60 Hz, including six rigid-body modes. The 52 mode shapes, frequencies, and generalized masses resulting from that analysis were used as an input to the current study. The orientation and position of each mirror were represented by considering the motion of three node points selected on each mirror; for example, translations of nodes 1, 21, and 15 serve to define the orientation and the location of the secondary mirror, as well as providing three degrees of freedom of deformation.

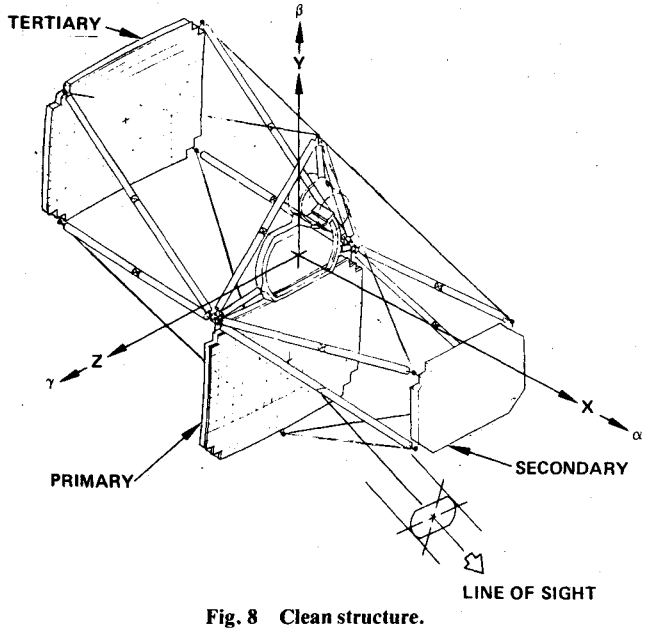

Fig. 8 Clean structure.

Table 1 shows the frequencies of the first 52 modes which were determined by the Stardyne analysis. These modes do not all have the same significance for the optical performance. For example, several low-frequency modes occur in pairs which represent vibrations of the tension cables. These modes have a small generalized mass and have little effect on the relative motion of the principal optical elements. On the other hand, mode number 26 (at 7½ Hz) represents a large bending of the entire structure which involves relatively large motions of the mirrors and consequent large effects on the line of sight. In assembling the total system model, a method of truncation was used in which the coupling characteristics of the modes were taken into account as well as the frequencies. The simplest flexible model of the optics which was used is one in which the motions consist of relative motions of the mirrors. (These were derived from the Stardyne output data but were not explicit natural modes of the system.) After design with this model, modes were added to the simulations and frequency responses to represent further coupling. These were found to have little effect on the line-of-sight error because they do not produce significant relative motion of the mirrors.

Figure 9 represents the attitude control system model. In keeping with the philosophy of testing the simplest configuration, the pitch-roll and yaw loops were all regarded as independent. The attitude sensors were located on the secondary mirror, and attitude torques were applied by reaction wheels on the dirty box. No explicit attitude rate measurement was used, and a second-order compensation was used in each channel. The compensation parameters were essentially established by a pole placement method using three separate one-degree-of-freedom rigid models of the entire spacecraft. The frequencies were picked to be 0.05 Hz for each of the closed-loop rigid models. The inertial coupling between the three loops was ignored, but the best success was

Table 1 Mode frequencies of the structure

Number	Frequency, Hz	Number	Frequency, Hz
1	0.00	27	9.10
2	0.00	28	9.12
3	0.00	29	9.12
4	0.00	30	9.14
5	0.00	31	9.73
6	0.00	32	10.09
7	4.66	33	10.73
8	4.71	34	10.80
9	5.18	35	10.88
10	5.24	36	11.02
11	5.24	37	12.29
12	5.25	38	12.35
13	5.96	39	12.45
14	5.96	40	12.57
15	5.99	41	14.26
16	6.04	42	15.07
17	6.47	43	19.65
18	6.66	44	24.05
19	6.68	45	25.98
20	6.71	46	34.56
21	6.71	47	36.09
22	6.73	48	40.92
23	6.75	49	45.47
24	6.79	50	46.92
25	6.84	51	50.82
26	7.50	52	56.09

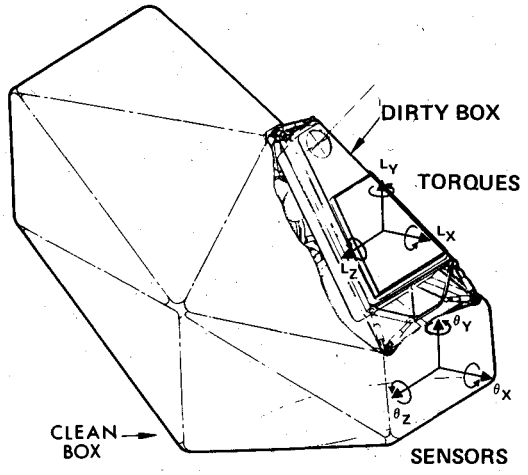

Fig. 9 Attitude control.

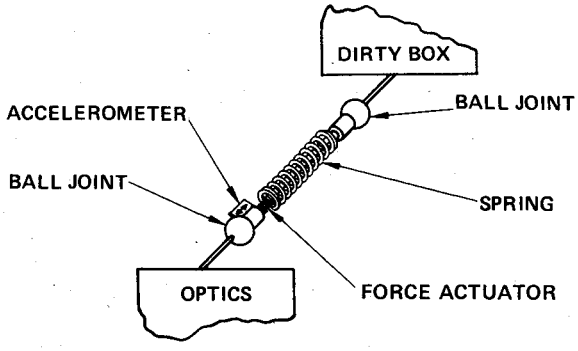

Fig. 10 Isolator model detail.

achieved when the sensors and the reaction wheels were aligned very nearly with system principal axes, so the dynamic coupling was small.

Figure 10 illustrates the isolation concept in detail as applied to this system. The isolator consists of a force actuator in parallel with a spring. It applies a force only along the axis of the spring. Each isolator was connected by a ball joint at one end to the dirty box and by a ball joint at the other end to the optics. The six isolators are used in pairs, with two isolators connected to each of three points on the optics. The orientation of the two was such that they were separated by an angle of 90 deg in their common plane. The planes of the three pairs of isolators were then chosen so that the optics module did not have any rigid-body degrees of freedom relative to the dirty box. The feedback loop in each isolator consisted of an accelerometer measuring the inertial acceleration on the optics side, an integrator, and a force proportional to the output of the integrator. In the system model, the integrator and the accelerometer were modeled as an inertial velocity measurement along the axis of the isolator.

For this study, the design of the attitude control system was accomplished by first choosing attitude control loop parameters so that good low-bandwidth performance was achieved using a model in which everything was rigid. Then the isolation degrees of freedom were freed allowing six flexible modes due to the isolation springs between a rigid representation of the optics and a rigid representative of the dirty box. Isolation feedback gain which provided adequate performance with this model was determined, and then additional flexible degrees of freedom of the optics were included in the simulation and frequency response analyses. The additional flexible degrees of freedom, as predicted, did not introduce any significant departures in the overall character of the performance except to provide resonances at the expected frequencies.

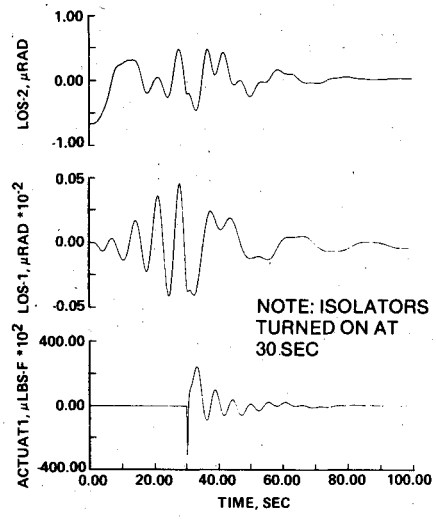

Fig. 11 Transient response.

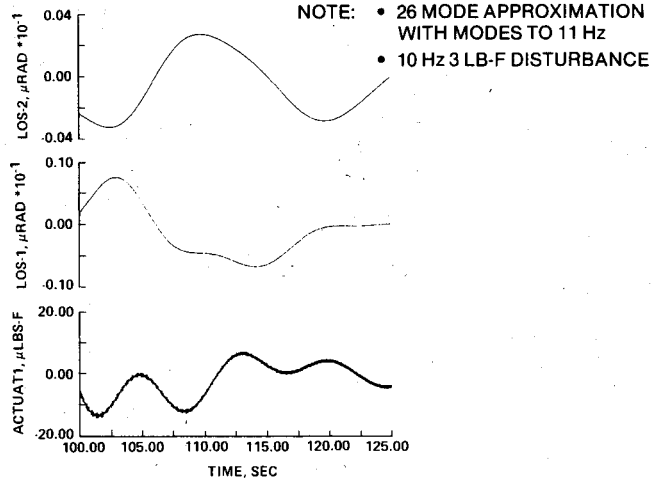

Fig. 12 Isolator force and line-of-sight error response to disturbance.

System Performance Results

Figure 11 illustrates transient response with and without isolation. The system was given a microradian attitude error at time 0. This does not reflect as a full microradian line-of-sight error because the line-of-sight axes were skewed relative to the attitude reference axes in the simulation. The isolation system was not turned on at the beginning of the simulation, and for the attitude control parameters used in this particular simulation, the motion was unstable without the active isolation. At 30 s, the isolator was turned on and motion was stabilized. The isolation gain used in the feedback in this particular simulation was relatively low, so the oscillation takes several cycles to be damped out.

Figure 12 shows the time response to a disturbance force on the dirty box. To obtain these results, the simulation was run with only low-frequency modes included in the model for 80 s. This allowed relatively inexpensive simulation of the damping of the principal attitude transient due to the turn-on of the disturbance at time 0. Additional flexible modes were then added which resulted in a relatively small transient of these modes and a slight perturbation of the overall attitude motion. The results shown here from 100 to 125 s are based on a 26-mode approximation of the system, including the large structural flexing mode at 7½ Hz. The disturbance was a 10 Hz, 3-lb force acting on the dirty box. The actuator forces are responding at the 10 Hz frequency, but the 10 Hz oscillation in the line of sight is too small to be distinguished on the curves here.

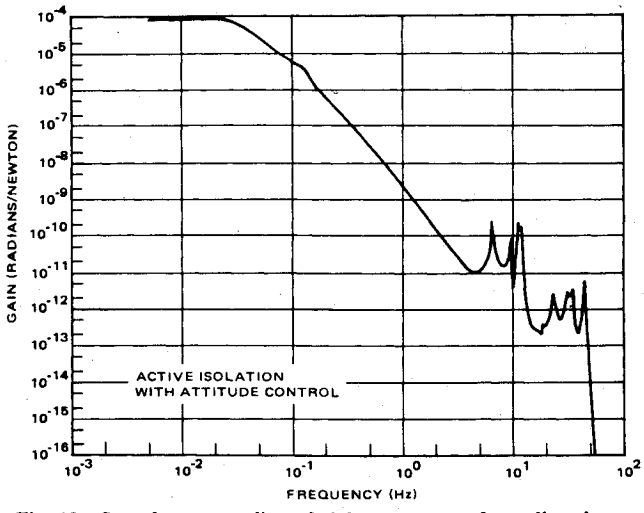

Fig. 13 Sample output—line-of-sight response to force disturbance.

A typical frequency response of line of sight to disturbance force is shown in Fig. 13. The disturbance input here was a force in a direction parallel to the surface of the vibrating equipment module as shown in Fig. 1. The output is the line-of-sight γ amplitude (Fig. 8). The frequency response is the same at low frequencies as that shown in Fig. 7. It breaks downward at the attitude control frequency of 0.05 Hz, and at 0.1 Hz, the isolator frequency, there is a second break downward. The response then decreases at approximately 80 dB per decade. By the time structural resonances are reached, the effect of the force on the line of sight is down many orders of magnitude.

In order to compare active isolation with passive isolation, an acceleration input was used instead of a force input. These results are shown in Fig. 14. There are a number of interesting things to note about these figures. First of all, the response of the active loop is much the same with the acceleration input as with a force input. The passive system responds to relative velocity between the dirty box and the clean box, so at the isolation frequency there is a rise due to the resonance. The most significant difference is the asymptotic slope of the curve as discussed previously. A third feature that is apparent in these curves is of some significance. The active isolation system has a significant damping effect on the structural modes within the optical system. This is evidenced by the fact that the structural resonance peaks are significantly smaller for the active loop.

Conclusions

A simple isolation concept based on local feedback of local measurements has been presented. The results show that this isolation approach, which is relatively insensitive to detailed modeling, has significant potential for achieving high levels of optical performance. This method is applicable to many cases in which the vibrating equipment can be adequately modularized as a dirty box. While there are many details of the application which have not been explored, analysis of a realistic model of both the line-of-sight dependence on the flexible motions and the system dynamics shows that the method is worthy of serious consideration.

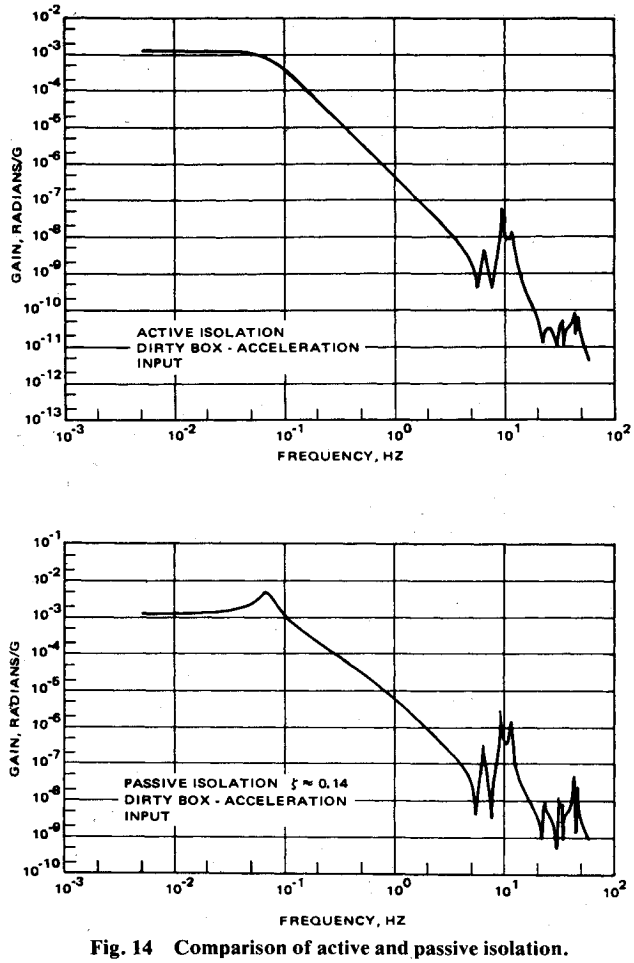

Fig. 14 Comparison of active and passive isolation.

Acknowledgments

This work was performed as part of an IR&D study at Hughes Aircraft Company.

References

[1] Yocum, J.F. and Slafer, L.I., "Control System Design in the Presence of Severe Structural Dynamics Interactions," *Journal of Guidance and Control,* Vol. 1, March-April 1978, pp. 109-116.

[2] Ruzicka, J.E. and Derby, T.F., *Influence of Damping in Vibration Isolation,* The Shock and Vibration Monograph Series SUM-7, Naval Research Laboratory Shock and Vibration Center, Washington, D.C., 1971.

[3] Karnopp, D., Crosby, N.J., and Harwood, R.A., "Vibration Control Using Semi Active Force Generators," *Journal of Engineering for Industry,* May 1974, p. 619.

[4] Sevin, E. and Pilkey, W.D., *Optimum Shock and Vibration Isolation,* The Shock and Vibration Monograph Series SUM-6, Naval Research Laboratory Shock and Vibration Center, Washington, D.C., 1971.

[5] Balas, M.J. and Canavin, J.R., "An Active Modal Control System Philosophy for a Class of Large Space Structures," presented at AIAA Symposium on Dynamics and Control of Large Flexible Spacecraft, Virginia Polytechnic Institute, Blacksburg, Va., June 1977.